journal homepage: www.intl.elsevierhealth.com/journals/cmpb

Fall detection for multiple pedestrians using depth image processing technique

*Shih-Wei Yang**, *Shir-Kuan Lin*

Institute of Electrical and Control Engineering, National Chiao Tung University, Hsinchu, Taiwan

ARTICLE INFO

Article history:
Received 29 September 2013
Received in revised form
28 January 2014
Accepted 5 February 2014

Keywords:
Fall detection
Depth image analysis
Multiple pedestrian detection
Illumination compensation

ABSTRACT

A fall detection method based on depth image analysis is proposed in this paper. As different from the conventional methods, if the pedestrians are partially overlapped or partially occluded, the proposed method is still able to detect fall events and has the following advantages: (1) single or multiple pedestrian detection; (2) recognition of human and non-human objects; (3) compensation for illumination, which is applicable in scenarios using indoor light sources of different colors; (4) using the central line of a human silhouette to obtain the pedestrian tilt angle; and (5) avoiding misrecognition of a squat or stoop as a fall. According to the experimental results, the precision of the proposed fall detection method is 94.31% and the recall is 85.57%. The proposed method is verified to be robust and specifically suitable for applying in family homes, corridors and other public places.

1. Introduction

The accidental fall is a common high-risk injury, especially with regard to the elderly and the physically disabled. Therefore, communities for the elderly, hospitals and other public places are becoming required to install fall detection systems. The most common fall detection techniques can be divided into two types. The first type is such that the pedestrian wears at least one sensor which gathers the information related to changes in the posture of the user. Then, the fall event is judged according to the acquired information of wearable sensors [1–6]. Abbate et al. [7] designed a fall detection system embedded in a smart phone, and thus the smart phone could detect walking, falling and lying down events. However, the wearable sensors may inconvenience the movement of the elderly and the physically disabled. Moreover, if the user forgets to wear the sensors, these methods are completely ineffective.

The second type is the visual surveillance. The two-dimensional (2D) images are captured by a monocular camera, and are used for detecting whether the pedestrian has fallen through the image processing technique [8–13]. Liao et al. [14] combined the features of pedestrians with a Bayesian Belief Network model to detect slip-only events and fall events. However, when more than two pedestrians are partially overlapped, the above 2D methods are likely to cause misjudgments or even completely inapplicable. The depth camera systems [15–19] can be used for solving the occlusion problem. The stereo vision techniques of multi-cameras [16,17] have been proposed for fall detection, but the resulted computation is often huge. The fall detection system based on a Time-of-Flight sensor [18] provides the precise depth information and the guaranty of people privacy, while the system

* *Corresponding author*. Tel.: +886 3 5712121x54423.
E-mail address: swyang.nctu@msa.hinet.net (S.-W. Yang).

http://dx.doi.org/10.1016/j.cmpb.2014.02.001
0169-2607/

setup is very expensive. Rougier et al. [19] obtain the pedestrian centroid height relative to the ground by a structured light sensor (Microsoft Kinect [20]) for detecting falls, but the proposed algorithm is only suitable for detecting a single person and cannot recognize a fall from brutally sitting down or squatting.

Therefore, this study proposes a fall detection technique using the Kinect sensor, which is low cost, so as to improve the above drawbacks. By analyzing the captured depth images, the proposed method identifies a single pedestrian or mutually overlapped pedestrians, and determines whether each pedestrian has fallen. As different from the ellipse fitting technique [14,21], a simplified algorithm of human shape analysis for calculating the pedestrian tilt angle is proposed. In addition, some suitable solutions which can be integrated with the proposed method to enhance the people privacy are also discussed in Section 2. According to the experimental results, the proposed method can distinguish falls, squats and other highly similar motions, thus, avoiding the misjudgments effectively.

2. Methods of fall detection for multiple pedestrians

2.1. Foreground extraction and overlapped object segmentation

As the position of the depth camera is fixed, a depth image of the background is built first, so that each of subsequent depth images can be subtracted from this background image. This allows the system to segment the foreground and background, and the segmentation results can be expressed as a binary image (Fig. 1):

$$g_{xy} = \begin{cases} 255, & \left|z_{xy} - z_{xy(b)}\right| \geq T_b \\ 0, & \left|z_{xy} - z_{xy(b)}\right| < T_b \end{cases} \quad (1)$$

where g_{xy} is the gray value of pixel (x,y) in the binary image; $z_{xy(b)}$ is the depth value of pixel (x,y) in the background image; z_{xy} is the depth value of pixel (x,y) in the ith frame; T_b is the binary threshold of depth value.

The segmentation results of Eq. (1) are more accurate than using the color image; the error resulting from the foreground and background colors being too similar can be avoided.

There may be overlapped objects in any isolated area of the foreground, as shown in Fig. 1 (point cloud data). Therefore, the concept of clustering is used to segment overlapped objects:

Step 1 The depth value of every pixel in the isolated area is sorted in ascending order to obtain a depth sequence. The differences D_{21}, D_{32},..., $D_{i(i-1)}$,..., $D_{n(n-1)}$ between two consecutive depths in the sequence are calculated, where n denotes the total number of pixels in this isolated area.

Step 2 Ignore the zero differences, and let the average value μ of the minimal non-zero difference and the maximal non-zero difference be the initial threshold. All the non-zero differences are divided by μ into two groups. Those smaller than μ are the first group and the average value μ_1 is calculated; those greater than or equal to μ are the second group and the average μ_2 is calculated. Last, the new threshold $\mu_{new} = (\mu_1 + \mu_2)/2$ is calculated. If μ is equal to μ_{new}, μ is the depth threshold for segmenting overlapped objects; otherwise, let $\mu = \mu_{new}$ and repeat this step until μ converges.

Since there may be a slight depth gap in the pixels of a single object, a threshold T_c is set, and $T_c = 30$ (mm) in this paper. T_c denotes the minimum distance between two overlapped objects that need to be segmented. If $\mu < T_c$, it is not necessary to segment this isolated area. However, if $\mu \geq T_c$ and $D_{i(i-1)} \geq \mu$, as shown in Fig. 2(a), this isolated area contains two overlapped objects. The pixels with a depth value less than or equal to the $(i-1)$th depth value in the sequence are regarded as one object, while the pixels with depth value greater than or equal to the ith depth value in the sequence are regarded as another object. The segmentation of overlapped objects is shown in Fig. 2 (b). This method is also applicable to the segmentation of more than three overlapped objects.

2.2. Human object detection

After segmentation, if any object has enough skin colored pixels, the object is recognized as a pedestrian. To avoid the result of skin color detection being influenced by a non-white light source, the illumination compensation should be taken before skin color detection. According to the Gray World Assumption [22,23], the average values of R, G and B components of an image without color deviation should be very close to each other. Therefore, if the image fails to meet the above condition, the R, G and B components of every pixel are corrected to:

$$R'_{xy} = \begin{cases} 255, & R_{xy} \geq R_{5\%} \\ R_{xy} \times \dfrac{255}{R_{5\%}}, & R_{xy} < R_{5\%} \end{cases} \quad (2)$$

$$G'_{xy} = \begin{cases} 255, & G_{xy} \geq G_{5\%} \\ G_{xy} \times \dfrac{255}{G_{5\%}}, & G_{xy} < G_{5\%} \end{cases} \quad (3)$$

$$B'_{xy} = \begin{cases} 255, & B_{xy} \geq B_{5\%} \\ B_{xy} \times \dfrac{255}{B_{5\%}}, & B_{xy} < B_{5\%} \end{cases} \quad (4)$$

where R'_{xy}, G'_{xy} and B'_{xy} are the R, G and B components of pixel (x,y) after compensation; R_{xy}, G_{xy} and B_{xy} are the R, G and B components of pixel (x,y) before compensation; $R_{5\%}$, $G_{5\%}$ and $B_{5\%}$ are the lower bounds of the top 5% R, G and B components of the image.

The silhouette of each object is corresponded to the color image after illumination compensation, and the nonlinear skin color detection method from Ref. [23] is used to calculate the number of skin colored pixels of each object (see [23] for details). As long as an object has a skin colored area of 10% or over, it is recognized as a pedestrian and labeled with

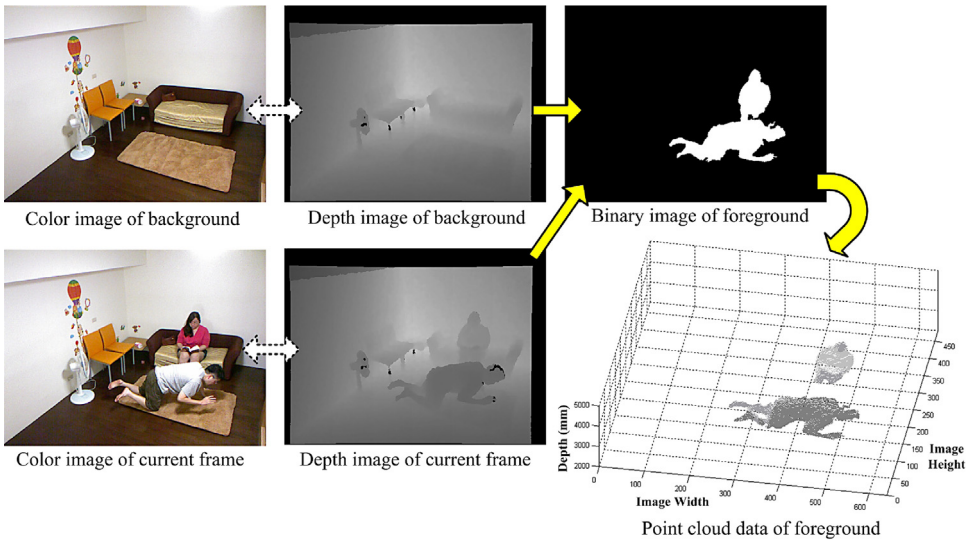

Fig. 1 – Foreground extraction using depth images.

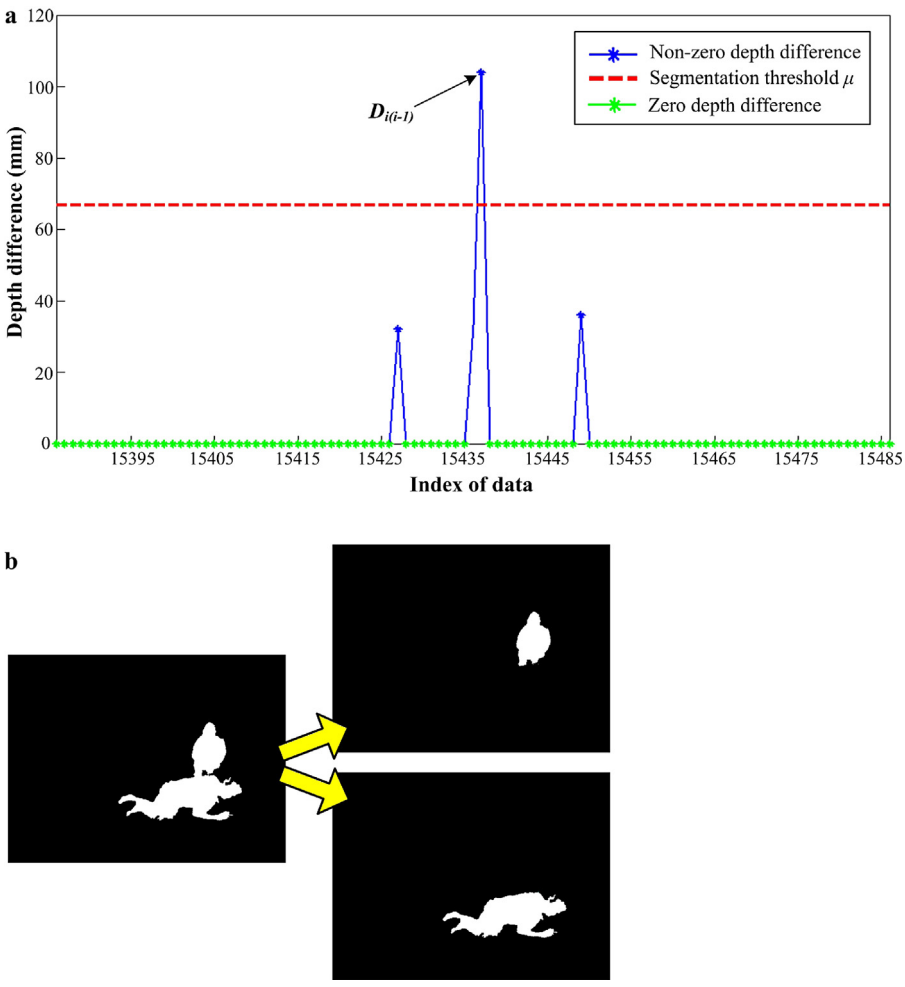

Fig. 2 – (a) Process of depth value clustering and (b) result of overlapped objects segmentation.

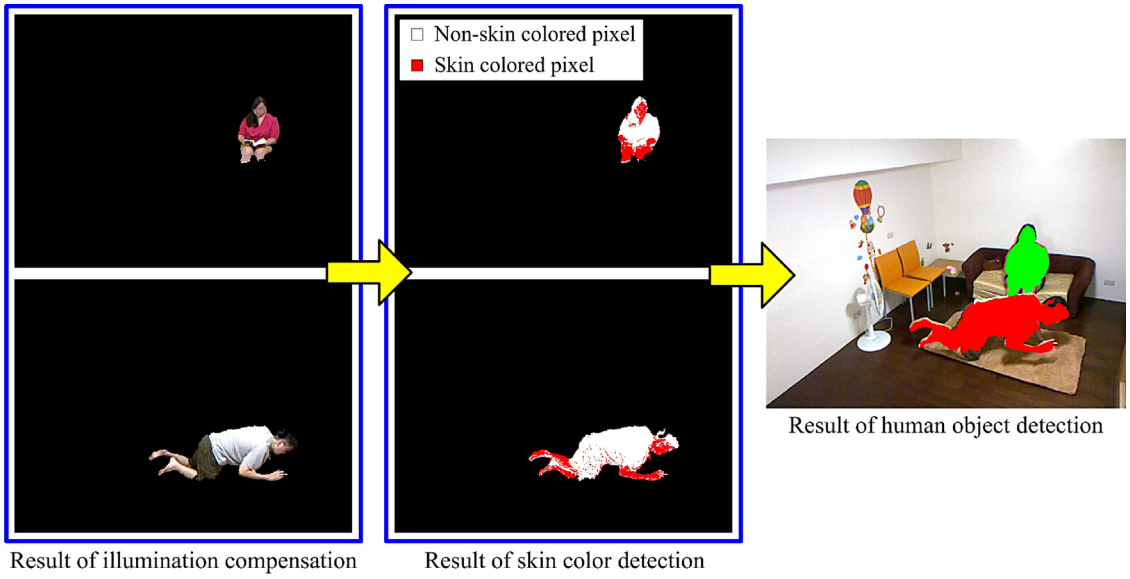

Fig. 3 – Process of human object detection.

a specific color for tracking; otherwise, it is ignored, as shown in Fig. 3.

2.3. *Human object tracking*

The three-dimensional (3D) centroid of each pedestrian in the real world coordinate system is calculated for object tracking. Since the definition of a real world coordinate system is different from the definition of the projective coordinate system of the captured image, and the units of X- and Y-axis are also different, as shown in Fig. 4(a), the 3D centroid of pedestrians must be converted before tracking. Let the vertical field of view of camera be FOV_v (degree), and horizontal field of view be FOV_h (degree). Take the XZ plane as an example, following the concept that the depth value z_{xy} of any point in a real world coordinate is equal to that in projective coordinates, as shown in Fig. 4(b). The 3D centroid of a pedestrian in the real world coordinate system can be derived as:

$$\begin{cases} x' = \left(\frac{x}{w} - 0.5\right) \times z_{xy} \times 2 \ \tan\left(\frac{FOV_h}{2}\right) \\ y' = \left(0.5 - \frac{y}{h}\right) \times z_{xy} \times 2 \ \tan\left(\frac{FOV_v}{2}\right) \\ z' = z_{xy} \end{cases} \quad (5)$$

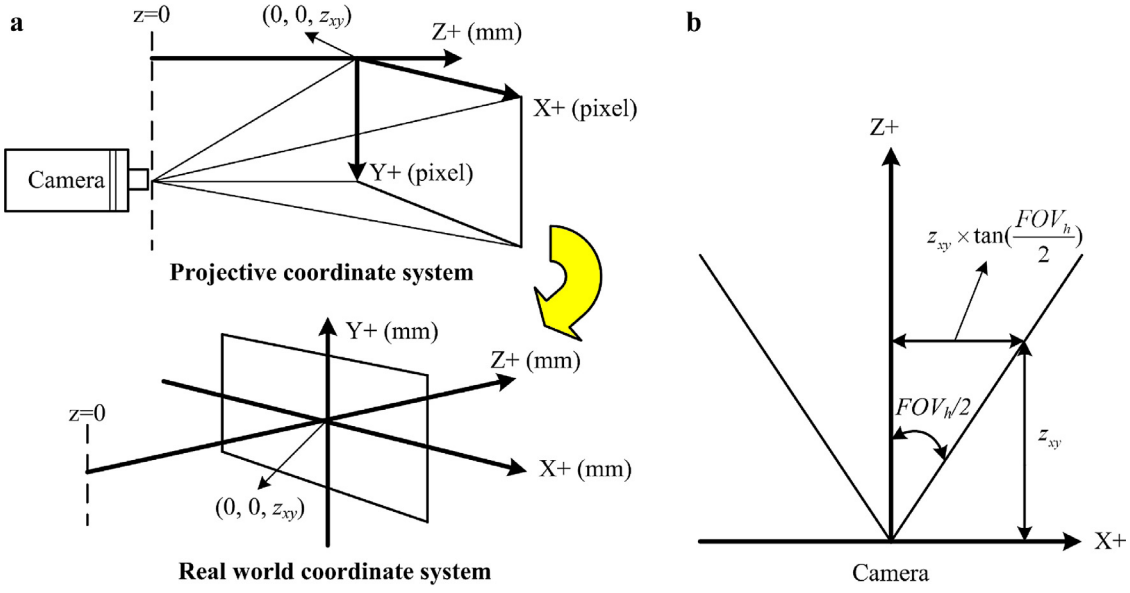

Fig. 4 – (a) Difference of the real world coordinate system and the projective coordinate system and (b) correlation of two coordinate systems in XZ plane.

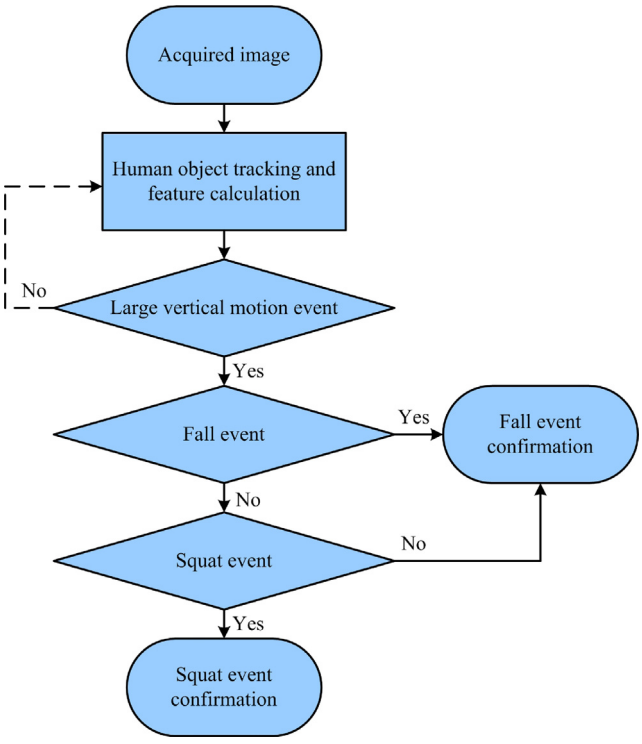

Fig. 5 – Flowchart of the proposed fall and squat detection method.

where (x', y', z') is the pedestrian centroid of real world coordinate system; (x, y, z_{xy}) is the pedestrian centroid of projective coordinate system; $w \times h$ is the image resolution.

Every pedestrian centroid of previous frame will be mapped to the current frame according to the shortest distance between two centroids. The owner of a specific pair of centroids is regarded as the same pedestrian in the consecutive images.

2.4. *Fall and squat detection*

To avoid misjudging stoop and squat motions as falls, the flowchart of proposed fall and squat detection method is illustrated in Fig. 5. The required features are calculated and saved continuously after tracking.

2.4.1. *Large vertical motion event*

During the course of a fall, the y coordinate y_c (the projective coordinate is directly used) of a pedestrian centroid forms an increasing sequence. The starting point ($y_{c(x)}$) of this sequence is the moment when the fall begins and the end point ($y_{c(e)}$) of this sequence is the moment when the fall ends, as shown in Fig. 6. The images at these two moments are used to judge the occurrence of every event in Fig. 5.

When the following two equations are satisfied at the same time, this means a large vertical motion event occurs:

$$y_{c(e)} - y_{c(s)} \geq \frac{H_{(s)}}{4} \tag{6}$$

$$H_{(s)} - H_{(e)} \geq \frac{H_{(s)}}{3} \tag{7}$$

where $y_{c(s)}$ denotes the centroid y coordinate when the pedestrian starts falling; $y_{c(e)}$ denotes the centroid y coordinate when the pedestrian ends falling; $H_{(s)}$ denotes the silhouette height when the pedestrian starts falling; $H_{(e)}$ denotes the silhouette height when the pedestrian ends falling.

Eqs. (6) and (7) show that only if the pedestrian centroid has obvious vertical displacement and the pedestrian silhouette height has clearly changed, the occurrence of a large vertical motion event is identified. This event implies that someone probably has fallen. Then, it is required to be recognized as a fall event or squat event; otherwise, the proposed system does not execute fall detection. Note that Eq. (6) will not be satisfied when a pedestrian stoops, and Eq. (7) will not be satisfied if a pedestrian only walks vertically in front of the camera, hence avoiding other misjudgments.

2.4.2. *Fall event*

An initiated ray starts from the pedestrian centroid $C(x_c, y_c)$ towards the edge of a human silhouette and is rotated by fixed angle θ each time for 360° scanning, as shown in Fig. 7(a). The equation of any initiated ray is:

$$\begin{cases} x_e = x_c + r\ \cos\theta \\ y_e = y_c + r\ \sin\theta \end{cases} \tag{8}$$

where $E(x_e, y_e)E$ is the sampled edge point that initiated ray passes through; $r > 0$; $0 < \theta \leq 2\pi$.

The two initiated rays at angles θ and $(\theta + 180°)$ are combined into a straight line, the equation of this straight line can be expressed as $y_e = x_e \tan\theta + (y_c - x_c \tan\theta)$. The minimum distance d between a sampled edge point and this straight line is calculated as:

$$d = \left| \frac{x_e\ \tan\theta - y_e + (y_c - x_c\ \tan\theta)}{(\tan^2\theta + 1)^{1/2}} \right| \tag{9}$$

where the range of θ becomes $(0,\pi]$.

The distances between all the sampled edge points and the straight lines corresponding to different θ are summed up, and the straight line of a minimum sum is defined as a central line. The angle between the central line and Y-axis is defined as the pedestrian tilt angle θ_t. It is worth pointing that the precision of the derived pedestrian tilt angle depends on the value of selected θ, and $\theta = 5°$ in this paper.

The tilt angle $\theta_{t(s)}$ when the pedestrian begins to fall and the tilt angle $\theta_{t(e)}$ when the fall ends are determined, as shown in Fig. 7(b). When $\theta_{t(e)} - \theta_{t(s)} \geq T_f$, a fall event is identified. Where T_f is a preset threshold, and $T_f = 45°$ in this paper. Otherwise, the squat event detection will be executed.

2.4.3. *Squat event*

Sometimes a pedestrian may fall backward directly onto the ground, this kind of fall motion is very similar to a squat. However, a squat is an autonomous motion. In general, a

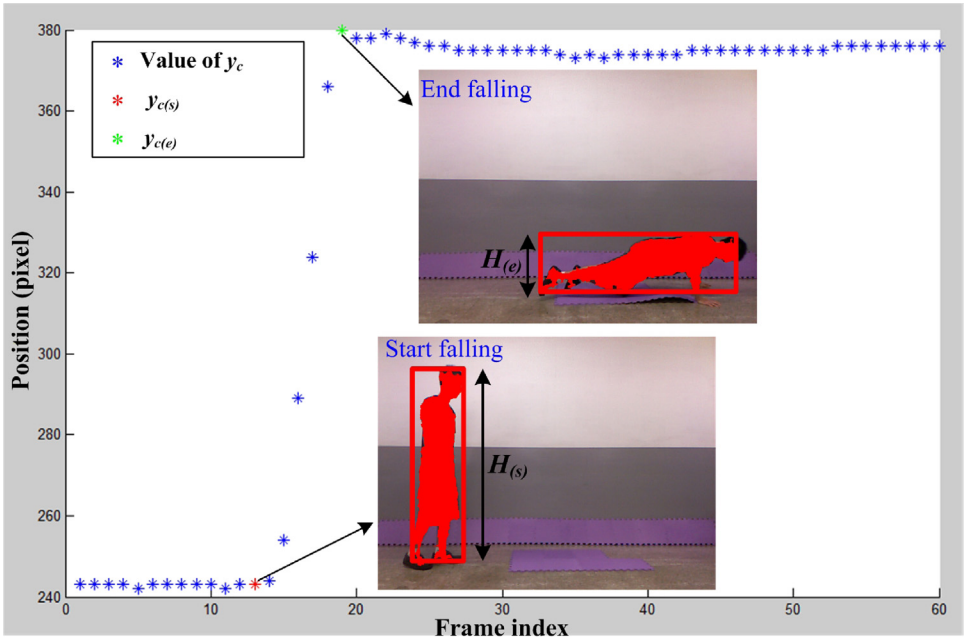

Fig. 6 – Y-axis position of pedestrian centroid during falling.

pedestrian squats more slowly than they fall. For this reason, when a large vertical motion event occurs whereas and a fall event does not occur, the pedestrian may squat or fall backward onto the ground. The vertical velocity of pedestrian centroid v_c in the period from the beginning of the pedestrian fall to the end of the fall in Fig. 6 is calculated. When $v_c \geq T_v$, a fall event is identified. Where T_v is a preset threshold, and $T_v = 12$ pixels/frame in this paper. Otherwise, the pedestrian just squats and a squat event is identified.

3. Experimental results and discussion

3.1. *Experimental setup of the proposed fall detection method*

The Kinect sensor is adopted for acquiring the depth images in this study, and the depth information is estimated through the projected infrared structure light (see [20] for details). The resolution of the captured images is 640 × 480, and the average

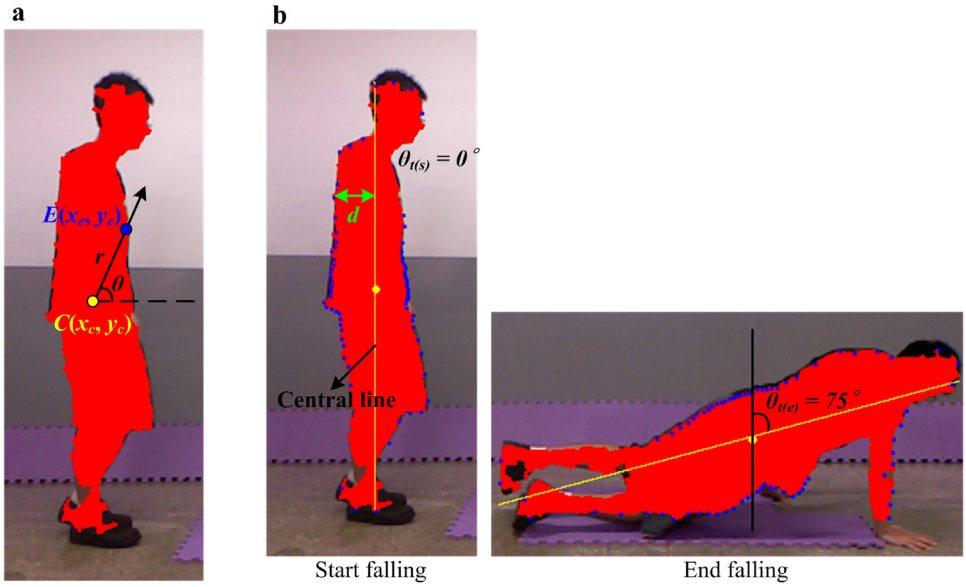

Fig. 7 – (a) Sampled edge points of human silhouette and (b) the obtained tilt angles for fall event detection.

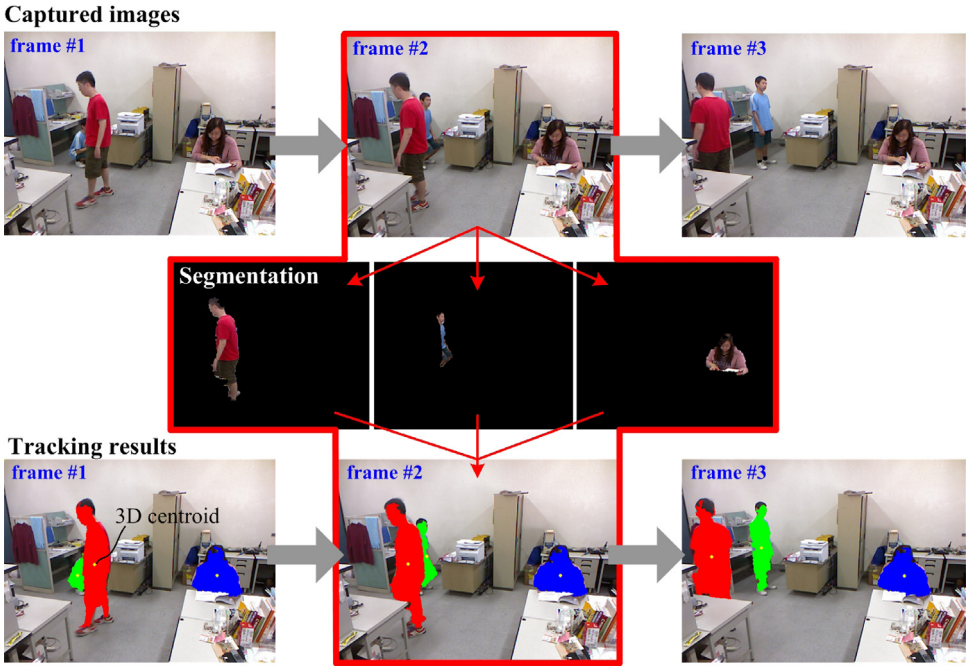

Fig. 8 – The results of proposed segmentation and tracking steps in a complex background.

processing rate of proposed system is 10–15 fps. After overlapped object segmentation, if a same object meets the rules of Section 2.2 in 10 consecutive frames, this object is identified as a pedestrian. Each pedestrian is tracked with the 3D centroid in the real world coordinate system, and the features x_c, y_c, H and θ_t are continuously recorded. An example of how the proposed segmentation and tracking steps react in a complex background is shown in Fig. 8. Once a large vertical motion event is identified, the features of a pedestrian begins to fall and ends falling are used to detect fall events and squat events.

For surveillance purpose, a wall-mounted setup is usually adopted for its good effect of limiting the occlusions. While in some scenarios of the following experiments, the Kinect sensor is also mounted closer to the ground plane, in order to verify the ability of proposed method for detecting the falls of the occluded or overlapped pedestrians. In each experiment, two important factors are used to evaluate the accuracy of the proposed fall detection method:

$$\text{Precision} = \frac{tp}{tp + fn} \times 100\% \tag{10}$$

$$\text{Recall} = \frac{tp}{tp + fn} \times 100\% \tag{11}$$

where tp (true positive) denotes the number of fall events or squat events detected in the experiment and which actually occurred; fp (false positive) denotes the number of fall events or squat events detected in the experiment but did not occur, i.e. false alarms; fn (false negative) denotes the number of fall events or squat events not detected in the experiment but did occur.

Note that a higher precision represents a lower probability of misjudgments, and a higher recall implies that the detected omission will occur less likely.

3.2. *Experimental results and details of the automatic fall detection*

Five cases were simulated in different scenarios including the home-like environments and the corridors to validate the accuracy of the proposed method, and various motions such as forward falls, backward falls, sideward falls, squats, stoops and sitting down actions were tested. In every case, multiple pedestrians are detected according to the algorithm of Fig. 5, and the conditions of the overlapped pedestrians with and without occlusion are specifically analyzed in Case #3 and #4. The status of each pedestrian in the scenario is highlighted with different colored bounding rectangles (fall detection for multiple pedestrians), i.e. the fall event is labeled with red, the squat event is labeled with green, and the normal state is labeled with white. The experimental results of five simulated cases are illustrated as follows:

Case #1: Two non-overlapped pedestrians fall forward, fall backward, squat, stoop and sit down.
This case is used to illustrate that the proposed fall detection method is applicable to non-overlapped pedestrians, as shown in Fig. 9(a). By the proposed method, a fall event can still be detected successfully in a complex background according to Fig. 9(b). Note that Eqs. (6) and (7) are not satisfied at the same time when the pedestrian stoops, squats or sits down, hence these motions will not be misjudged as a fall event, as shown in Fig. 9(c) and (d). The experimental results of Case #1 are shown in Table 1.
Case #2: A yellow light is used as the source of indoor illumination.
In the case of non-white lighting, the illumination compensation is applied to the color image so as to guarantee the accuracy of skin color detection results. Fig. 9(e) shows

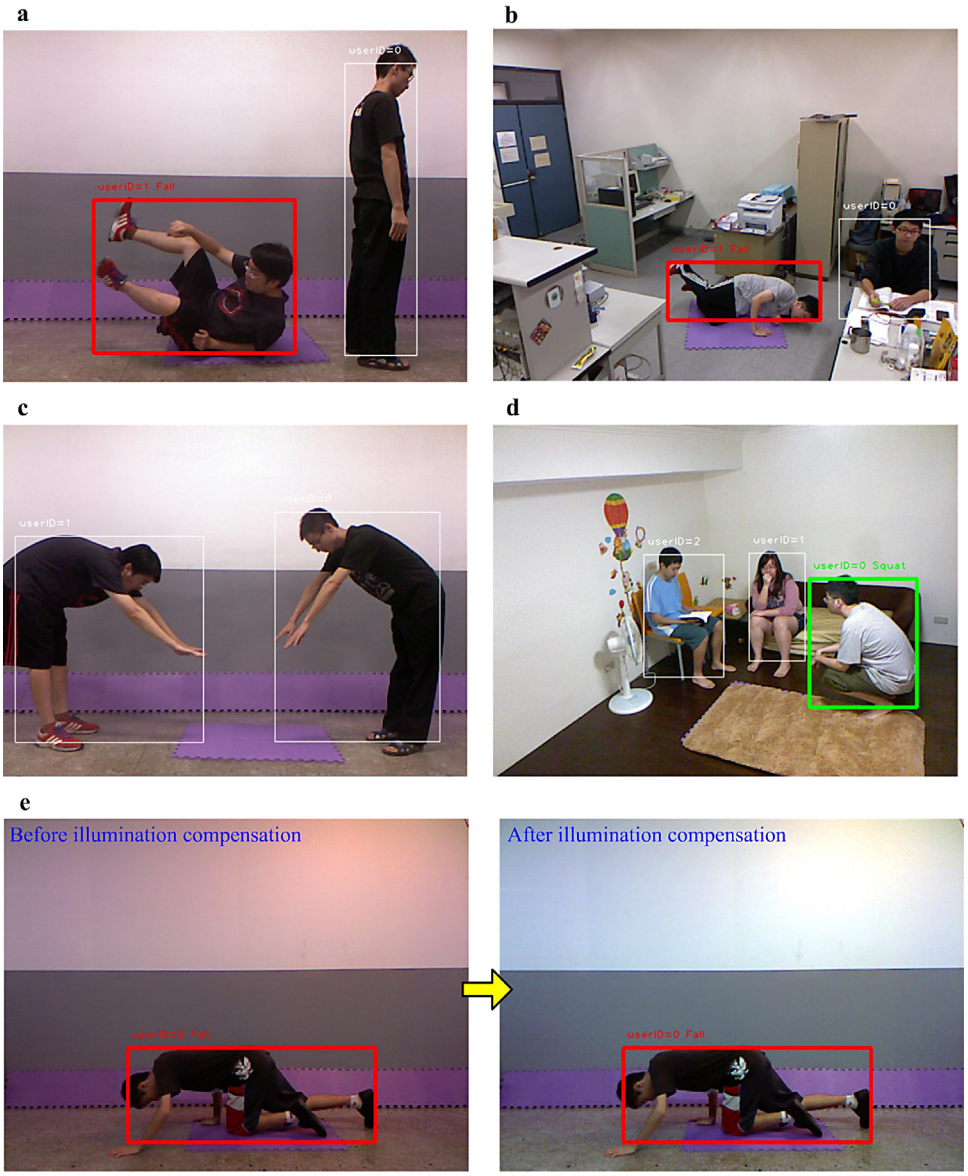

Fig. 9 – (a) A fall event of a non-overlapped pedestrian in the corridor is detected, (b) a fall event of a non-overlapped pedestrian in the complex background is detected, (c) the stoop motions are not misjudged as the fall events, (d) the sitting down actions and the squat event are not misjudged as the fall events, and (e) the color images before and after illumination compensation.

Table 1 – Experimental results of Case #1.

	Number of fall events	Number of squat events
Ground truth	14	6
tp	14	6
fp	0	0
fn	0	0
Precision	100%	100%
Recall	100%	100%

Table 2 – Experimental results of Case #2.

	Number of fall events	Number of squat events
Ground truth	25	9
tp	23	9
fp	0	2
fn	2	0
Precision	100%	81.82%
Recall	92%	100%

Table 3 – Experimental results of Case #3.

	Number of fall events	Number of squat events
Ground truth	9	8
tp	9	8
fp	0	0
fn	0	0
Precision	100%	100%
Recall	100%	100%

the image before illumination compensation and the results after illumination compensation. According to Fig. 9(e), this method can avoid misjudging the non-human object as a pedestrian under the yellow light. The experimental results of Case #2 are shown in Table 2.

Case #3: One of the overlapped pedestrians who is not occluded falls and squats.

When two pedestrians are partially overlapped, the pedestrian closer to the camera is not occluded; this case is used to evaluate the fall detection effect under the above condition. As long as the distance between the pedestrians is larger than the depth resolution of the camera, the overlapped pedestrians can be successfully segmented through the method in Section 2.1, and the status of each pedestrian in the scenario is individually recognized, as shown in Fig. 10(a). Another example containing multiple detected events in a home-like environment is given in Fig. 10(b), and the experimental results of Case #3 are shown in Table 3.

Case #4: A partially occluded pedestrian falls and squats.

When the pedestrians are overlapped and the occluded area is not large, the proposed method is still accurate, as shown in Fig. 10(c). However, if the occluded area is too large, the pedestrian cannot be recognized as a human object, this may lead a detection failure. Sometimes the Kinect sensor feeds back abnormal background depth values, resulting in an incorrect object segmentation result which will cause a false alarm, as shown in Fig. 10(d). The experimental results of Case #4 are shown in Table 4.

Case #5: One of the overlapped pedestrians falls sideways.

As the field of view of camera is parallel to the falling direction of pedestrians, i.e. when the camera is mounted closer to the ground, and a pedestrian falls sideways, the variance in θ_t may be very small. In such a case, the determination of a fall event and squat event depends on the vertical velocity v_c of the pedestrian centroid. A successfully detected sideward fall is shown as Fig. 10(e). While using a wall-mounted camera, the sideward fall can still be detected through the variance of the pedestrian tilt angle, as shown in Fig. 10(f). Note that if a pedestrian falls sideways overlapping another pedestrian and the distance between the two persons and the camera is too close to the maximal detection distance, the two pedestrians are possibly misjudged as the same person due to the poor depth resolution at the region too far from the sensor, and the fall event cannot be detected correctly. The experimental results of Case #5 are shown in Table 5, and the experimental results of five cases are summarized in Table 6.

Table 5 – Experimental results of Case #5.

	Number of fall events
Ground truth	36
tp	26
fp	4
fn	10
Precision	86.67%
Recall	72.22%

3.3. *Discussion of the experimental results*

The proposed system is much simpler for installation and calibration than the multi-cameras system [16,17], and can obtain the depth images of higher resolution than a Time-of-Flight sensor [18] with a lower cost. When comparing with Ref. [19], the proposed method is able to segment the overlapped pedestrians and then detect whether each pedestrian has fallen separately; while the method in Ref. [19] simply segments the foreground object from the background image without further checking the overlapping situation, and is only applicable to the scenario with a single pedestrian. Moreover, the proposed technique of calculating the pedestrian tilt angle is simplified and straightforward. In comparison with the ellipse fitting method [14,21], the processing time can be reduced by adjusting the value of θ.

According to the experimental results, the proposed fall detection method has good accuracy, not only overcoming the problem of pedestrian overlapping and occlusion, but also having applicability in scenarios involving indoor light sources of different colors. The result of squat event detection verifies that the proposed method can recognize the falls from the similar motions robustly and thus avoiding misjudgments. In addition, the proposed method can be modified simply to preserve the pedestrian privacy by only displaying the colored mask (e.g. Fig. 8) as the detected results. Other image processing techniques [24] such as blur, silhouette, or bounding-box can also be integrated with the proposed method to fulfill the goal of privacy enhancements.

Table 4 – Experimental results of Case #4.

	Number of fall events	Number of squat events
Ground truth	13	5
tp	11	4
fp	1	0
fn	2	1
Precision	91.67%	100%
Recall	84.62%	80%

Table 6 – Experimental results of Case #1–5.

	Number of fall events	Number of squat events
Ground truth	97	28
tp	83	27
fp	5	2
fn	14	1
Precision	94.31%	93.1%
Recall	85.57%	96.43%

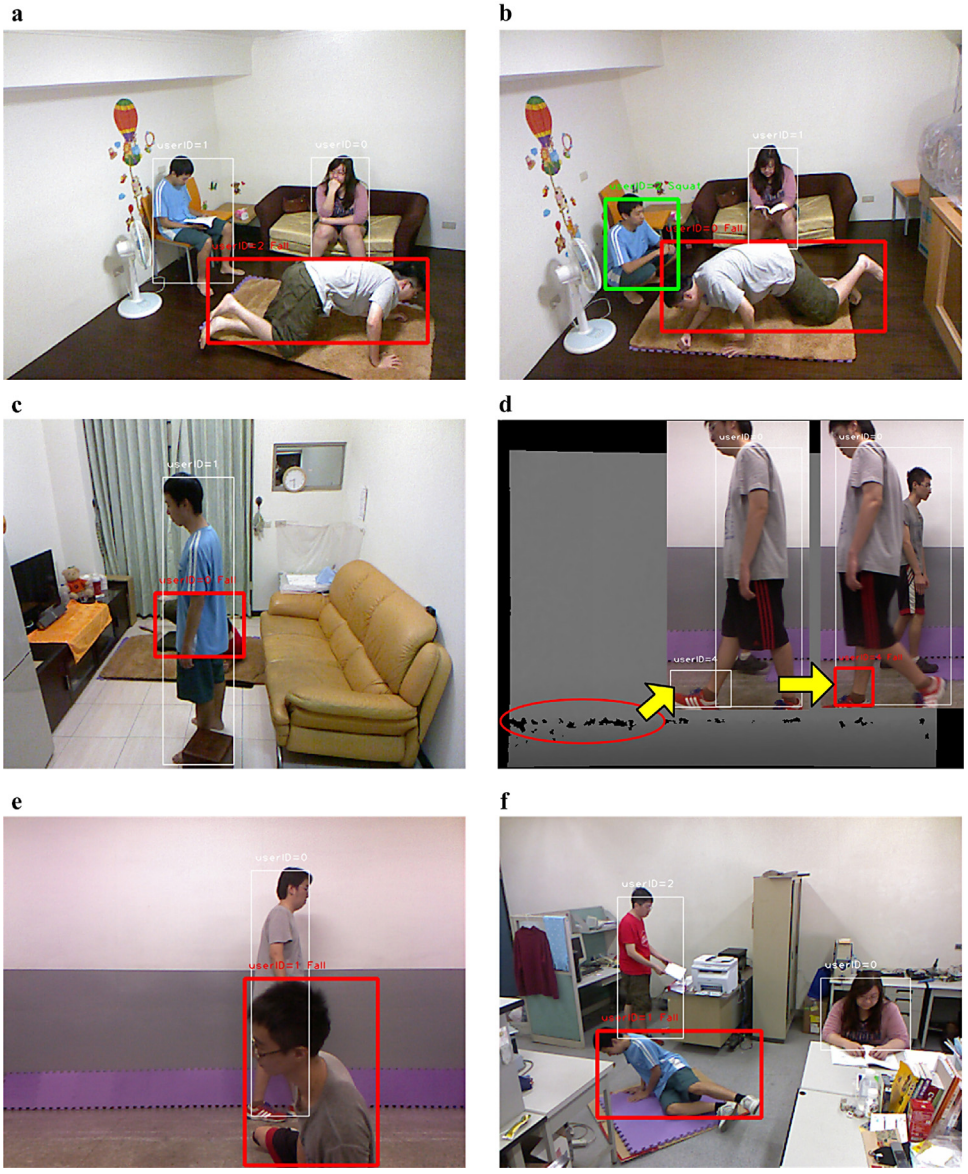

Fig. 10 – (a) A fall event in the scenario of multiple pedestrians is detected, (b) a fall event and a squat event are detected simultaneously, (c) a fall event of a partially occluded pedestrian is detected, (d) a false alarm due to the returned depth error of background, (e) a sideward fall is detected through the vertical velocity of the pedestrian centroid, and (f) a sideward fall is detected through the variance of the pedestrian tilt angle.

It should be noted that one of the main limitations of Kinect sensor is the depth resolution declines as the detection distance increases, in other words, the depth information is not always accurate for regions far from the sensor. The maximal detection distance of accurate depth information is suggested to be 5 meters after several tests. Another intrinsic limitation is the view of the depth image is adjusted to be consistent with the color image through view correction, thus the depth of boundary pixels in the depth image cannot be correctly retrieved. While in general, the precision and recall of proposed method are not affected severely by these boundary pixels. Only when the pedestrian falls exactly at the boundary region of the captured image, the abnormal depth values may possibly lead to a misjudgment.

4. Conclusions

In this paper, the depth image and color image were analyzed to detect fall events and squat events, especially in cases where pedestrians are partially overlapped and occluded. The pedestrian tilt angle was obtained by searching the central line of a human silhouette and was used as a main feature for fall detection. The vertical velocity of a pedestrian was also used to determine fall events and squat events. According to the experimental results, the proposed method demonstrated the ability to effectively avoid misjudging squat and stoop motions as falls, and the fall detection precision and recall are good when the pedestrians were overlapped and occluded.

The proposed algorithm can be easily implemented for other applications using a different camera with proper depth resolution and depth detection distance.

Acknowledgment

This work was sponsored by the National Science Council under Grant No. NSC 102-2221-E-009-064.

REFERENCES

[1] M.N. Nyan, F.E.H. Tay, E. Murugasu, A wearable system for pre-impact fall detection, Journal of Biomechanics 41 (2008) 3475–3481.
[2] T. Klingeberg, M. Schilling, Mobile wearable device for long term monitoring of vital signs, Computer Methods and Programs in Biomedicine 106 (2) (2012) 89–96.
[3] A.K. Bourke, G.M. Lyons, A threshold-based fall-detection algorithm using a bi-axial gyroscope sensor, Medical Engineering & Physics 30 (2008) 84–90.
[4] E.E. Tripoliti, A.T. Tzallas, M.G. Tsipouras, G. Rigas, P. Bougia, M. Leontiou, S. Konitsiotis, M. Chondrogiorgi, S. Tsouli, D.I. Fotiadis, Automatic detection of freezing of gait events in patients with Parkinson's disease, Computer Methods and Programs in Biomedicine 110 (1) (2013) 12–26.
[5] C.F. Lai, S.Y. Chang, H.C. Chao, Y.M. Huang, Detection of cognitive injured body region using multiple triaxial accelerometers for elderly falling, IEEE Sensors Journal 11 (3) (2011) 763–770.
[6] F. Büsching, U. Kulau, M. Gietzelt, L. Wolf, Comparison and validation of capacitive accelerometers for health care applications, Computer Methods and Programs in Biomedicine 106 (2) (2012) 79–88.
[7] S. Abbate, M. Avvenuti, F. Bonatesta, G. Cola, P. Corsini, A smartphone-based fall detection system, Pervasive and Mobile Computing 8 (2012) 883–899.
[8] M. Mubashir, L. Shao, L. Seed, A survey on fall detection: principles and approaches, Neurocomputing 100 (2013) 144–152.
[9] M. Pediaditis, M. Tsiknakis, N. Leitgeb, Vision-based motion detection, analysis and recognition of epileptic seizures—a systematic review, Computer Methods and Programs in Biomedicine 108 (3) (2012) 1133–1148.
[10] W. Ludwig, K.H. Wolf, C. Duwenkamp, N. Gusew, N. Hellrung, M. Marschollek, M. Wagner, R. Haux, Health-enabling technologies for the elderly—an overview of services based on a literature review, Computer Methods and Programs in Biomedicine 106 (2) (2012) 70–76.
[11] D.N. Olivieri, I.G. Conde, X.A.V. Sobrino, Eigenspace-based fall detection and activity recognition from motion templates and machine learning, Expert Systems with Applications 39 (2012) 5935–5945.
[12] C. Rougier, J. Meunier, A. St-Arnaud, J. Rousseau, 3D head tracking for fall detection using a single calibrated camera, Image and Vision Computing 31 (3) (2013) 246–254.
[13] P.J. Figueroa, N.J. Leite, R.M.L. Barros, A flexible software for tracking of markers used in human motion analysis, Computer Methods and Programs in Biomedicine 72 (2) (2003) 155–165.
[14] Y.T. Liao, C.L. Huang, S.C. Hsu, Slip and fall event detection using Bayesian Belief Network, Pattern Recognition 45 (2012) 24–32.
[15] X. Yu, Approaches and principles of fall detection for elderly and patient, in: 10th International Conference on e-Health Networking, Applications and Services, 2008, pp. 42–47.
[16] E. Auvinet, F. Multon, A. St-Arnaud, J. Rousseau, J. Meunier, Fall detection with multiple cameras: an occlusion-resistant method based on 3D silhouette vertical distribution, IEEE Transactions on Information Technology in Biomedicine 15 (2) (2011) 290–300.
[17] N. Thome, S. Miguet, S. Ambellouis, A real-time, multiview fall detection system: a LHMM-based approach, IEEE Transactions on Circuit and Systems for Video Technology 18 (11) (2008) 1522–1532.
[18] G. Diraco, A. Leone, P. Siciliano, An active vision system for fall detection and posture recognition in elderly healthcare, in: Design, Automation and Test in Europe Conference and Exhibition, 2010, pp. 1536–1541.
[19] C. Rougier, E. Auvinet, J. Rousseau, M. Mignotte, J. Meunier, Fall detection from depth map video sequences, in: 9th International Conference on Toward Useful Services for Elderly and People with Disabilities: Smart Homes and Health Telematics, 2011, pp. 121–128.
[20] Microsoft Kinect. http://www.microsoft.com/en-us/kinectforwindows/
[21] C. Rougier, J. Meunier, A. St-Arnaud, J. Rousseau, Fall detection from human shape and motion history using video surveillance, in: 21st International Conference on Advanced Information Networking and Applications Workshops, Vol. 2, 2007, pp. 875–880.
[22] E.Y. Lam, Combining gray world and retinex theory for automatic white balance in digital photography, in: Proceedings of the Ninth International Symposium on Consumer Electronics, 2005, pp. 134–139.
[23] R.L. Hsu, M. Abdel-Mottaleb, A.K. Jain, Face detection in color images, IEEE Transactions on Pattern Analysis and Machine Intelligence 24 (5) (2002) 696–706.
[24] A. Edgcomb, F. Vahid, Accurate and efficient algorithms that adapt to privacy-enhanced video for improved assistive monitoring, ACM Transactions on Management Information Systems 4 (3) (2013), No. 14.